Journal of Magnetic Resonance **146,** 110–121 (2000)
doi:10.1006/jmre.2000.2143, available online at http://www.idealibrary.com on IDEAL®

Multiphoton Resonances in Pulse EPR

I. Gromov[1] and A. Schweiger

Laboratory for Physical Chemistry, ETH-Zentrum, Swiss Federal Institute of Technology, CH-8092, Zurich, Switzerland

E-mail: schweiger@esr.phys.chem.ethz.ch

Received December 27, 1999; revised April 11, 2000

Two- and three-photon electron spin echoes of a two-level system are observed using, in addition to the microwave excitation, a linearly polarized radio-frequency field oriented along the static magnetic field B_0. Such multiphoton echoes are detected when the sum of the energies of one microwave and one or two radio-frequency photons are equal to the difference between energies of two spin states. The multiphoton character of the echoes is confirmed by measuring the spin nutation frequency as a function of the angle between the radio-frequency field and B_0, and monitoring the echo amplitude as a function of the radiation field strengths. Floquet theory, usually applied for the description of multiphoton resonances with an odd number of photons, is extended to the case where an even number of photons participate in the transition.

Key Words: **multiphoton resonance; electron spin echo; pulse EPR; dressed states; Floquet theory.**

INTRODUCTION

The interaction of electromagnetic radiation with matter, where several photons are simultaneously absorbed or emitted, is the physical basis of many effects, as Raman scattering, multiphoton absorption and emission, multiphoton ionization, and harmonic generation (*1*). Such multiphoton resonances predicted during the first half of this century (*2*) are now widely applied in coherent optics (*3*). In EPR and NMR multiphoton resonances have been known for a long time, but have not yet been used as spectroscopic tools extensively.

Quantum mechanics requires that the energy, as well as the total angular momentum, is conserved in any transition process. As a consequence, to induce multiphoton transitions in magnetic resonance, the number, the polarization, and the energy of photons involved in the transition must be in accordance with the total change in spin angular momentum and spin energy at the end of the transition.

In continuous wave (cw) magnetic resonance spectroscopy, multiphoton transitions, where the magnetic spin quantum number changes by $\Delta m > 1$, have been observed in electron and nuclear *multilevel* spin systems with photons of the same or of different frequencies (*4–8*). It should be noted, for example, that in a system with nonmixed states the probability of a single-photon transition with $\Delta m = 2$ is zero, while for a two-photon transition, it is nonzero. The description of these kinds of multiphoton transitions is based on time-dependent perturbation theory and requires a real intermediate energy level (*9*).

In *two-level* systems with nuclear $I = \frac{1}{2}$ or electron $S = \frac{1}{2}$ spins, a $(2n + 1)$-photon transition with $\Delta m = 1$ requires $(n + 1)$ circularly polarized photons rotating in one direction and n circularly polarized photons rotating in the opposite direction. Intermediate spin states do not exist in *two-level* systems, and the explanation of the multiphoton resonances in this case is based on the concept of "dressed" atoms (*10*). Figure 1a shows an example for a three-photon magnetic resonance transition with two right-hand circularly polarized photons (σ^+ photons) and one left-hand circularly polarized photon (σ^- photon). In the case of an even number of photons, linearly polarized photons (π photons) are also required to induce a multiphoton magnetic resonance transition, as depicted in Fig. 1b for a two-photon transition.

The first evidence for the existence of multiphoton resonances in a two-level spin system was obtained from experiments with optically pumped atoms (*11*). The resonances were observed when the Zeeman splittings of nuclear sublevels were close to $2n\omega$ and $(2n + 1)\omega$, where n is an integer and ω is the angular frequency of the radiation field. These effects have been explained as absorption of an even or odd number of photons (*12*). Later second harmonics (frequency 2ω) of an $S = \frac{1}{2}$ system were observed with a bimodal cavity during irradiation by a microwave (mw) field of frequency $\omega = \omega_0/2$ tilted from the static magnetic field $\mathbf{B}_0$ (*13*).

Multiphoton transitions in two-level systems can also be created with several photons of different frequencies. In cw EPR experiments two-photon transitions have been observed on free radicals in solids, where one mw σ^+ photon and one radio-frequency (rf) π photon are absorbed simultaneously (*14*). In this experiment the rf field was oriented parallel and the mw field perpendicular to $\mathbf{B}_0$.

In another approach it was demonstrated that multiphoton

[1] On leave from MRS Laboratory, Kazan State University, 42008, Kazan, Russian Federation.

1090-7807/00 $35.00

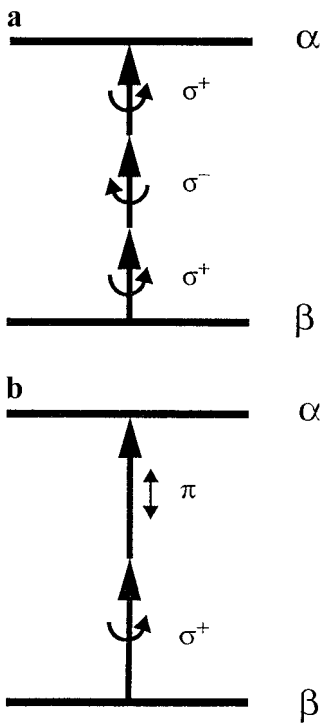

FIG. 1. Multiphoton transitions between the two states of an $S = \frac{1}{2}$ spin system in the static magnetic field B_0. (a) Three-photon transition induced by a right- and a left-hand circularly polarized field (σ^+ and σ^- photons). (b) Two-photon transition induced by a right-hand circularly polarized field (σ^+ photon) and a field which is linearly polarized (π photon) with respect to $\mathbf{B}_0$.

transitions can be induced by irradiating a two-level system with two closely spaced frequencies (bichromatic radiation) and using longitudinal detection for observation (*15, 16*). These experiments clearly demonstrate that a counterrotating field component is required for the observation of multiphoton transitions with an odd number of photons. In conventional single-photon, single-frequency magnetic resonance experiments, the counterrotating component is far off resonance and manifests only as a Bloch–Siegert shift (*17*) of the resonance line.

Recently, Hyde and co-workers introduced a cw EPR experiment where the spin system is saturated by two (or four) closely spaced mw frequencies (*18–21*). As in any nonlinear device, the spin system creates intermodulation sidebands, which can easily be detected (*18, 19*). Based on the dressed atom formalism and on Floquet theory the intermodulation sidebands have been explained as odd multiphoton resonances (*20, 21*).

A necessary condition for the excitation of multiphoton transitions is the nonlinear character of the interaction between the radiation field and the spin system. In many pulse magnetic resonance experiments a high radiation field is used, so that the response of the spin system is no longer linear. As examples, the nutation driven by a two-photon excitation in an $I = \frac{3}{2}$ system has been investigated by recording the polarization of a single-quantum transition (*22*), and bichromatic pulse excitation of double-quantum coherence of an $I = 1$ nuclear spin system has been studied (*23*). The evolution of an $I = \frac{1}{2}$ spin system under bi- and tetrachromatic radiation has been studied in detail both from the experimental and theoretical point of view (*24, 25*). An electron spin echo at the second harmonic was observed using an mw field tilted from the $\mathbf{B}_0$ direction and has been used to study the effect of spin diffusion on the spin dynamics (*26*). This experimental scheme also was used to monitor transient nutations in an $S = \frac{1}{2}$ system (*27*).

A multiphoton transition goes through a number of virtual states of the spin system, which correspond to the states of the system "dressed" by the electromagnetic field (*10*). Recently, the absorption of rf π photons by a spin system that evolves under the action of a strong resonant mw pulse was observed and has been used to carry out dressed spin-echo experiments (*28*).

Several theoretical approaches have been developed for the description of multiphoton processes (*29*). In magnetic resonance, multiphoton transitions are usually described by the Bloch equations (*22, 30, 31*), second quantization (*15, 16, 32*), and Floquet theory (*21, 24, 33*). The first two formalisms have been used to explain both even and odd multiphoton resonances, whereas Floquet theory, first implemented in spectroscopy by Shirley (*33*), has only been applied so far for the description of odd multiphoton resonances. Concurrently, it was demonstrated in NMR spectroscopy that Floquet theory is a powerful method for solving time-dependent problems (*34, 35*). The extension to many-mode Floquet theory allows one to describe the spin behavior under multifrequency radiation (*36*).

Multiphoton resonances in pulse EPR spectroscopy are very attractive from the point of view of spin dynamics and potential applications. In this work we show for the first time that even and odd multiphoton electron spin echoes created with radiation fields that differ in frequency by about three orders of magnitude can be observed, and that these experiments can be described using Floquet theory. After a brief review of the basics of Floquet theory, the formalism is applied to even multiphoton resonances. This takes the Floquet approach as a universal theoretical basis for the explanation of multiphoton experiments. The two-photon transition probabilities are evaluated numerically, and the relation between the transition rates and the strengths of the excitation fields is obtained by using perturbation theory, in the same way as used previously for the odd resonances (*24, 33*). Then, following the theory, new experiments are developed demonstrating that two- and three-photon electron spin echoes can be observed with an mw field perpendicular and an rf field parallel to $\mathbf{B}_0$.

FLOQUET THEORY

Floquet theory is a convenient method for solving Schrödinger's equation with periodic Hamiltonians. Since Floquet

theory is not frequently used in EPR investigations, we briefly review the approach following the work of Shirley (*33*) and extend the formalism to even multiphoton resonances.

Consider an $S = \frac{1}{2}$ electron spin system in a static magnetic field B_0 which is irradiated by a linearly polarized magnetic field $2B_1 \cos(\omega t)$. For an arbitrary angle $\theta = \angle(\mathbf{B}_0, \mathbf{B}_1)$, the laboratory frame Hamiltonian is given by

$$\mathcal{H}(t) = \omega_0 S_z + 2\omega_1 \cos(\omega t)[\cos(\theta) S_z + \sin(\theta) S_x], \quad [1]$$

where $\omega_0 = g\beta_e B_0/\hbar$ is the Larmor frequency, and $2\omega_1 = g\beta_e 2B_1/\hbar$ is the amplitude of the radiation field in angular frequencies. We denote the two eigenstates obtained for $\omega_1 = 0$ by α and β with $E_\alpha = \omega_0/2$ and $E_\beta = -\omega_0/2$.

To demonstrate the existence of multiple resonances, the transition probability $P_{\alpha\to\beta}$ of a system which evolves from the α state at time $t = 0$ to the β state under the Hamiltonian $\mathcal{H}(t)$ is calculated. For the prediction of the time dependence of the system, we introduce the time-evolution operator $U_{\alpha\beta}(t)$. For the matrix elements of a unitary operator $F(t)$, with $U(t) = F(t)F^{-1}(0)$, the time-dependent Schrödinger equation can then be written as a set of coupled equations

$$\frac{d}{dt} F_{\alpha\beta}(t) = -i \sum_\gamma \mathcal{H}_{\alpha\gamma}(t) F_{\gamma\beta}(t). \quad [2]$$

By applying the Floquet theorem for the solution of linear differential equations with periodic coefficients (*37*) we find for the solution of Eq. [2]

$$F_{\alpha\beta}(t) = \Phi_{\beta\alpha}(t) e^{-iq_\beta t}, \quad [3]$$

where $\Phi_{\beta\alpha}(t)$ are again periodic functions and q_β is the characteristic exponent. $F_{\alpha\beta}(t)$ in Eq. [3] and the Hamiltonian have the same periodic property, and both of them can be expanded in Fourier series

$$F_{\alpha\beta}(t) = \sum_n F^n_{\alpha\beta} e^{in\omega t} e^{-iq_\beta t}, \quad [4]$$

$$\mathcal{H}_{\alpha\beta}(t) = \sum_n \mathcal{H}^n_{\alpha\beta} e^{in\omega t}. \quad [5]$$

Substitution of these expansions into Eq. [2] and a rearrangement of the products of the Fourier series result in an infinite set of coupled equations for the matrix elements of the operator $F(t)$

$$\sum_{\gamma k} (\mathcal{H}^{n-k}_{\alpha\gamma} + n\omega\delta_{nk}\delta_{\alpha\gamma}) F^k_{\gamma\beta} = q_\beta F^n_{\alpha\beta}, \quad [6]$$

where the summation over k is taken from zero to n. This set has the form of a secular equation for an operator with eigenvalues q_β and eigenvectors with components $F^k_{\gamma\beta}$. The operator denoted by Shirley as the Floquet Hamiltonian is defined by

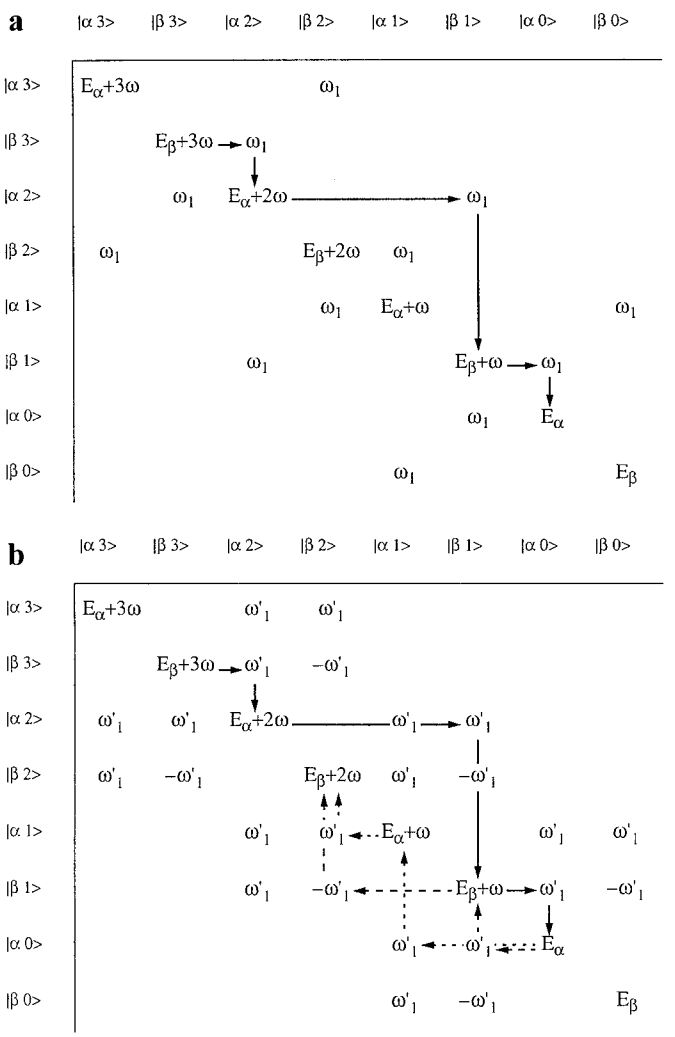

FIG. 2. Floquet Hamiltonians for an $S = \frac{1}{2}$ spin system and a single-frequency radiation field. (a) Radiation field perpendicular to the static magnetic field $\mathbf{B}_0$. (b) Radiation field tilted by 45° with respect to $\mathbf{B}_0$. The radiation field amplitude is ω_1, $\omega_1' = \omega_1/\sqrt{2}$. Pathways for multiphoton transitions: →, three-photon transitions $|\beta 3\rangle \to |\alpha 0\rangle$; – → - - - → two-photon transitions $|\beta 2\rangle \to |\alpha 0\rangle$.

$$\langle \alpha n | \mathcal{H}_F | \beta m \rangle = \mathcal{H}^{n-m}_{\alpha\beta} + n\omega\delta_{\alpha\beta}\delta_{nm}. \quad [7]$$

The expressions $|\alpha n\rangle$ represent Floquet states, α describes the spin state, and n denotes the Fourier component. Equation [7] and Fig. 2 indicate that the matrix elements of the Floquet Hamiltonian change periodically along the main diagonal and the three adjacent diagonals

$$\langle \alpha n + p | \mathcal{H}_F | \gamma l \rangle = \langle \alpha n | \mathcal{H}_F | \gamma l - p \rangle + p\omega\delta_{\alpha\gamma}\delta_{n(l-p)}. \quad [8]$$

As a consequence of the periodic structure of $\mathcal{H}_F$, the eigenvalues $\lambda_{\alpha n}$ will also be periodic

$$\lambda_{\alpha n+p} = \lambda_{\alpha n} + p\omega. \quad [9]$$

The property of the eigenvectors $|\lambda_{\gamma n}\rangle$ of $\mathcal{H}_F$ that belong to the eigenvalues $\lambda_{\gamma n}$ can be derived from the eigenvalue–eigenvector equation for $\mathcal{H}_F$ using Eqs. [8] and [9], revealing the periodic properties of the eigenvectors

$$\langle \alpha n + p|\lambda_{\beta m+p}\rangle = \langle \alpha n|\lambda_{\beta m}\rangle. \quad [10]$$

The characteristic exponent q_β is the same for each Fourier harmonic of the eigenvector components $F^n_{\alpha\beta}$ of eigenvalue q_β. Consequently, a connection between $\lambda_{\beta n}$ and q_β may be set as $\lambda_{\beta 0} = q_\beta$, which leads to the relation

$$F^n_{\alpha\beta} = \langle \alpha n|\lambda_{\beta 0}\rangle. \quad [11]$$

Substituting Eq. [11] into Eq. [4] results in an equation for the operator $F(t)$ and allows one to describe the time-evolution operator $U(t)$ for the semi-classical Hamiltonian in Eq. [1] in terms of the solution for the Floquet Hamiltonian in Eq. [7]

$$U_{\beta\alpha}(t) = \sum_n \sum_{\gamma l} \langle \beta n|\lambda_{\gamma l}\rangle e^{-i\lambda_{\gamma l}t}\langle \lambda_{\gamma l}|\alpha 0\rangle e^{in\omega t}. \quad [12]$$

Finally, the probability $\bar{P}_{\alpha\to\beta} = \langle U_{\beta\alpha}(t)U_{\beta\alpha}(t)^*\rangle_t$ averaged over time t can be obtained by integrating Eq. [12]

$$\bar{P}_{\alpha\to\beta} = \sum_n \sum_{\gamma l} |\langle \beta n|\lambda_{\gamma l}\rangle\langle \lambda_{\gamma l}|\alpha 0\rangle|^2. \quad [13]$$

Before calculating these transition probabilities, we must examine the Floquet matrices to get an idea about possible transitions between the Floquet states. Figure 2 shows parts of Floquet Hamiltonians, with $\mathcal{H}_F$ evaluated for $\theta = 90°$ (Fig. 2a) and $\theta = 45°$ (Fig. 2b). Figure 2a indicates that in the case of $\mathbf{B}_1 \perp \mathbf{B}_0$, the states $|\alpha n\rangle$ and $|\beta n + 1\rangle$ are connected by off-diagonal elements. A comparison of the Floquet theory with the second quantization approach reveals that the Fourier indices for the Floquet states correspond to the photon occupation number of the quantized radiation field (*10*, *33*). Thus, a transition $|\beta n + 1\rangle \to |\alpha n\rangle$ can be described as a spin flip from the β state to the α state with the absorption of one σ photon, representing a single-photon transition.

It can be seen from Fig. 2a that states which are distinguished by their spin projection and which differ in the number of photons by an odd value $m = 2l + 1$, where $l = 1, 2\ldots$, are indirectly coupled through $2l$ intermediate states. As an example, the three-photon transition $|\beta 3\rangle \to |\alpha 0\rangle$ is indicated by arrows in Fig. 2a. In the case of $\theta = 45°$ (Fig. 2b), state $|\alpha n\rangle$ is coupled with state $|\beta n + 1\rangle$ by a σ photon, and state $|\beta n + 1\rangle$ with state $|\beta n + 2\rangle$ by a π photon. The scheme indicates that transitions $|\beta n\rangle \to |\alpha n - m\rangle$, with $m = 2l$ are possible through $2l - 1$ intermediate states. As examples, the two possible pathways for the two-photon transition $|\alpha 0\rangle \to |\beta 2\rangle$ are indicated by broken lines.

The intensity of a multiphoton transition can be estimated by using the perturbation treatment developed in (*38*). In this approach the Floquet Hamiltonian is approximated by a 2×2 matrix $\mathcal{H}'_F$, whose diagonal elements have been corrected to take the remaining part of $\mathcal{H}_F$ into account, $\langle \gamma k|\mathcal{H}'_F|\gamma k\rangle = \langle \gamma k|\mathcal{H}_F|\gamma k\rangle \mp \delta_{\gamma k}$. Off-diagonal elements of $\mathcal{H}'_F$ can be considered as the effective radiation strength $\frac{1}{2}\omega^{(n-m)}_{\text{eff}}$ of the $(n - m)$ photon transition. For the matrix elements of $\mathcal{H}'_F$ one finds (*24*)

$$-\frac{1}{2}\omega^{(n-m)}_{\text{eff}} = \sum_{\gamma l} \frac{\langle \beta n|\mathcal{H}_F|\gamma l\rangle\langle \gamma l|\mathcal{H}_F|\alpha m\rangle}{E_{\beta n} - E_{\gamma l}} + \sum_{\gamma l}\sum_{\xi k} \frac{\langle \beta n|\mathcal{H}_F|\gamma l\rangle\langle \gamma l|\mathcal{H}_F|\xi k\rangle\langle \xi k|\mathcal{H}_F|\alpha m\rangle}{(E_{\beta n} - E_{\gamma l})(E_{\beta n} - E_{\xi k})} + \ldots, \quad [14]$$

and for the correction of the diagonal elements that introduces level shifts

$$\delta_{\beta n} = \sum_{\gamma l} \frac{\langle \beta n|\mathcal{H}_F|\gamma l\rangle\langle \gamma l|\mathcal{H}_F|\beta n\rangle}{E_{\beta n} - E_{\gamma l}} + \sum_{\gamma l}\sum_{\xi k} \frac{\langle \beta n|\mathcal{H}_F|\gamma l\rangle\langle \gamma l|\mathcal{H}_F|\xi k\rangle\langle \xi k|\mathcal{H}_F|\beta n\rangle}{(E_{\beta n} - E_{\gamma l})(E_{\beta n} - E_{\xi k})} + \ldots, \quad [15]$$

with $\gamma l, \xi k \neq \beta n, \alpha m$; $\gamma l \neq \xi k$; and $E_{\gamma l} = \langle \gamma l|\mathcal{H}_F|\gamma l\rangle$.

We assume that for an n-photon transition the Zeeman splitting is n times larger than the radiation frequency, $E_\alpha - E_\beta \approx n\omega$, and the strength of the oscillating field is weak, $\omega_1 \ll \omega$. For the three-photon transition $|\beta 3\rangle \to |\alpha 0\rangle$ shown in Fig. 2a we find for the effective field using Eq. [14]

$$\omega^{(3)}_{\text{eff}} = \frac{\omega_1^3}{2\omega^2} \quad [16]$$

and for the level shift in lowest order using Eq. [15]

$$\delta_{\beta 3} = -\delta_{\alpha 0} = -\frac{3\omega_1^2}{4\omega} \quad [17]$$

in agreement with Shirley (*33*). For the two-photon resonance $|\alpha 0\rangle \to |\beta 2\rangle$ shown in Fig. 2b with an oscillating field ω_1 inclined by an angle of 45° with the $\mathbf{B}_0$ field vector we obtain

$$\omega_{\text{eff}}^{(2)} = \frac{2\omega_1^2}{\omega}, \qquad [18]$$

and

$$\delta_{\beta 2} = -\delta_{\alpha 0} = -\frac{\omega_1^2}{3\omega}. \qquad [19]$$

Equation [18] demonstrates that the effective field for a two-photon transition is proportional to the square of the oscillating field strength and inverse proportional to the irradiation frequency; i.e., it shows the proportionality one would expect in going from three-photon resonances (Eq. [16]) to two-photon resonances. The dependences described by Eqs. [18] and [19] are the same as those found by solving the Bloch equations in the doubly rotating frame (*30*).

Equations [16] and [18] suggest that the corresponding $(n - m)$-photon transitions have nonzero transition probabilities. On the other hand these elements split the related eigenvalues $E_{\alpha m} = E_\alpha + m\omega$ and $E_{\beta n} = E_\beta + n\omega$, which are degenerated at the $(n - m)$-resonance condition $E_\alpha - E_\beta = (n - m)\omega$ when $\omega_1 = 0$. In the case of $\omega_1 \neq 0$, the level crossings ($E_{\alpha m} = E_{\beta n}$) are lifted. The unperturbed Floquet Hamiltonian $\mathcal{H}_F$ should correctly describe these level anticrossings. The existence of the multiphoton transitions thus implies a level anticrossing, and vice versa.

In order to demonstrate the existence of anticrossings we calculated the eigenvalues of the Floquet Hamiltonians evaluated with $\theta = 90°$ and 45° as a function of ω/ω_0 with $\omega_1/\omega_0 = 0.2$ and 14×14 Floquet Hamiltonian matrices (Figs. 3a, b). The calculation performed with $\theta = 90°$ reveals the existence of anticrossings at $\omega/\omega_0 = 0.38$, which corresponds to the position of a three-photon resonance (Fig. 3a). This result is in agreement with those previously reported (*24, 33*). The calculation for $\mathcal{H}_F(45°)$ demonstrates anticrossings in the vicinity of $\omega/\omega_0 = 1/n$, namely at $\omega/\omega_0 = 0.55$, 0.37, and 0.26, i.e., at the two-, three-, and four-photon resonances (Fig. 3b). Thus, one can expect that a radiation field tilted from $\mathbf{B}_0$ by 45° will induce even as well as odd resonances.

Numerical calculations of the time-averaged transition probability $\bar{P}_{\alpha\to\beta}$ using Eq. [13] were performed for $\mathcal{H}_F(90°)$ and $\mathcal{H}_F(45°)$ as a function of the normalized Larmor frequency ω_0/ω for field strengths $\omega_1/\omega = 0.25$, 0.5, and 0.75. To avoid effects caused by the limited dimension of the Hamiltonians, Floquet matrices of dimensions 42×42 were used in both cases, which cover resonances with up to 20 photons. The results for $\mathcal{H}_F(90°)$ (Figs. 4a, b, c) show odd resonances close to $\omega_0/\omega = (2n + 1)$, with $n = 0, 1, 2$, which move to lower ω_0/ω values when ω_1 increases, in agreement with the result reported in (*33*). In the case of $\mathcal{H}_F(45°)$ (Figs. 4d, e, f) the probability has maxima at approximately $\omega_0/\omega = n + 1$, with $n = 0, 1, \ldots, 4$, which demonstrates that with a tilted radiation field even resonances also appear in the spectrum.

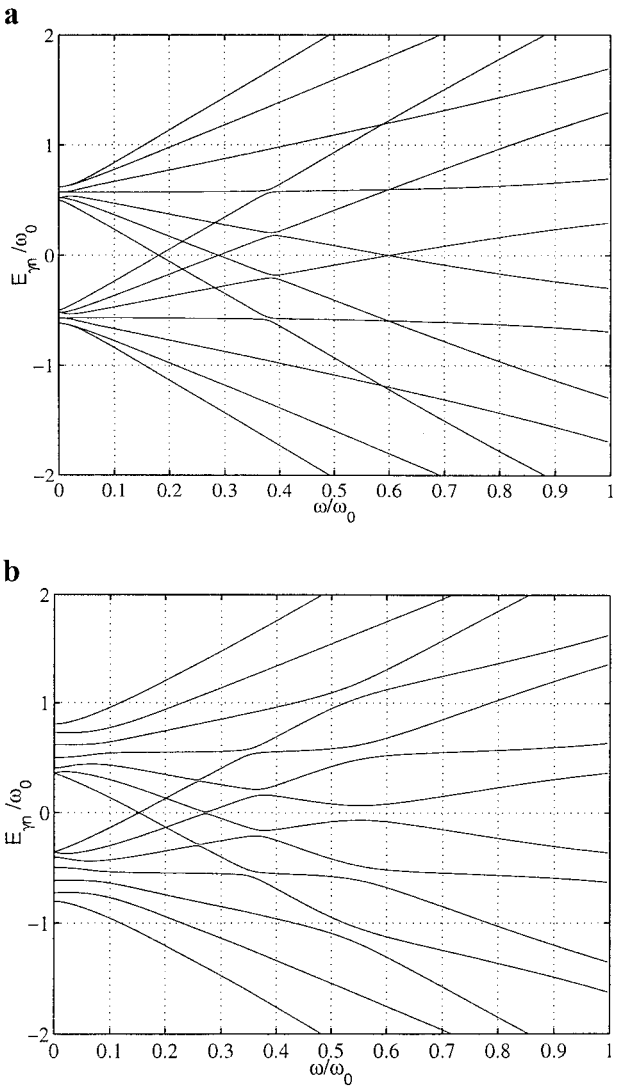

FIG. 3. Eigenvalues of the Floquet Hamiltonians in Fig. 2, calculated as a function of the normalized photon energy ω/ω_0 at $\omega_1/\omega_0 = 0.2$. (a) Eigenvalues for $\mathcal{H}_F$ ($\theta = 90°$). Anticrossings exist only near $\omega/\omega_0 = 0.37$ (apart from the single-photon resonances), which correspond to the position of the three-photon resonance. (b) Eigenvalues for $\mathcal{H}_F$ ($\theta = 45°$). Anticrossings are visible in the vicinity of $\omega/\omega_0 = 0.55$, 0.37, and 0.26, i.e., close to the two-, three-, and four-photon resonances.

The widths of the higher order resonances are extremely narrow at low values of ω_1 and broaden with ω_1, reflecting that energy levels at anticrossings become flatter at higher radiation fields.

Up to now we considered multiphoton resonances in which several photons with different polarization but with the same energy participate in the process. In this case the transitions go through a number of virtual levels (Floquet or dressed states), which are far away from a real energy level of the spin system (see Fig. 1). In single-frequency electron spin-echo experiments it is expected that the echoes of the two- and three-photon transitions will require relatively long excitation pulses

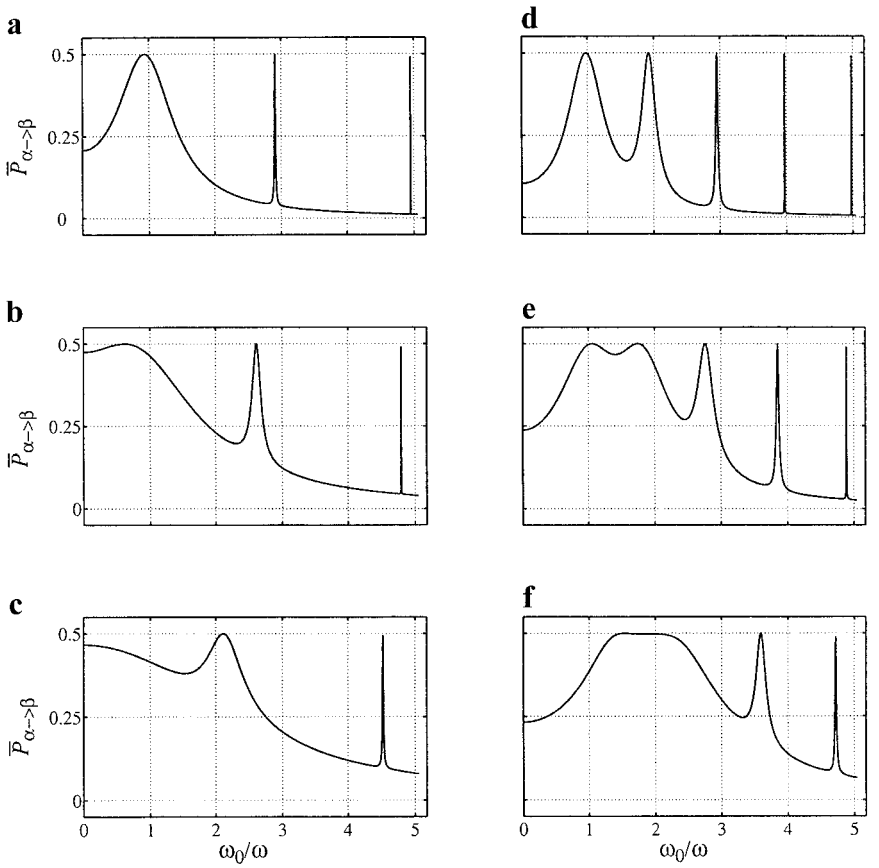

FIG. 4. Time-averaged transition probabilities evaluated from Eq. [13] as a function of the normalized electron Larmor frequency ω_0/ω, at different strength ω_1/ω of the radiation field: (a, d) $\omega_1/\omega = 0.25$, (b, e) 0.5, and (c, f) 0.75. (a, b, c) The radiation field is orthogonal to the static field. (d, e, f) The direction of the radiation field is tilted by 45° from $\mathbf{B}_0$.

or high radiation fields, since the effective field $\omega_{\text{eff}}^{(n-m)}$ is much weaker than that of a single-photon transition because in Eqs. [16] and [18] ω is in the denominator and is one-half or one-third of the Zeeman splitting. The situation can be considerably improved when the Floquet states are created in the vicinity of a real state. Such states can be generated, for example, by bi- or tetrachromatic radiation fields, which have components at frequencies close to the frequency of the single-photon transition (*15*, *20*, *25*).

For a two-photon resonance, virtual intermediate states can also be prepared by a transverse mw field with $\omega_{\text{mw}} \neq \omega_0$. An rf field with frequency $\omega_{\text{rf}} = \omega_0 - \omega_{\text{mw}}$ along $\mathbf{B}_0$ can then induce a transition with $\Delta m = 0$ between this virtual level and the real final state. This scheme has already been implemented for the observation of two-photon resonances in cw EPR (*14*). The same field configuration was used in dressed electron spin resonance, with the mw radiation on-resonance with the electron spins (*28*).

EXPERIMENTAL RESULTS

In this experimental section we present for the first time multiphoton electron spin echoes where an even and an odd number of photons are involved, and where the frequencies of the radiation fields differ by about three orders of magnitude. Figure 5a shows the field configuration in the laboratory frame with $\mathbf{B}_0$ (represented by ω_0) along z. The linearly polarized mw field with amplitude $2\omega_1$ and frequency ω_{mw} is oriented along y, and the linearly polarized rf field with amplitude $2\omega_2$ and frequency ω_{rf} lies in the xz plane with a variable angle θ.

The multifrequency experiments can be described by many-mode Floquet theory (*36*), but for simplicity we reduce the problem to the case of single-mode Floquet theory outlined above by applying a sequence of frame transformations. For $\theta = 0$ the laboratory frame Hamiltonian is given by

$$\mathcal{H}(t) = \omega_0 S_z + 2\omega_1 \cos(\omega_{\text{mw}} t) S_y + 2\omega_2 \cos(\omega_{\text{rf}} t) S_z. \quad [20]$$

$\mathcal{H}(t)$ is first transformed to the frame rotating at ω_{mw} around the z axis. In the rotating frame the effective static field $\omega_{\text{eff}} = (\omega_1^2 + \Omega_S^2)^{1/2}$, with $\Omega_S = \omega_0 - \omega_{\text{mw}}$, is tilted from z' by the angle ψ, with $\tan \psi = \omega_1/\Omega_S$. Then, neglecting the counterrotating mw component, a rotation around the x' axis by the angle ψ gives a new frame with z'' directed along the effective field. The Hamiltonian in this doubly primed frame becomes

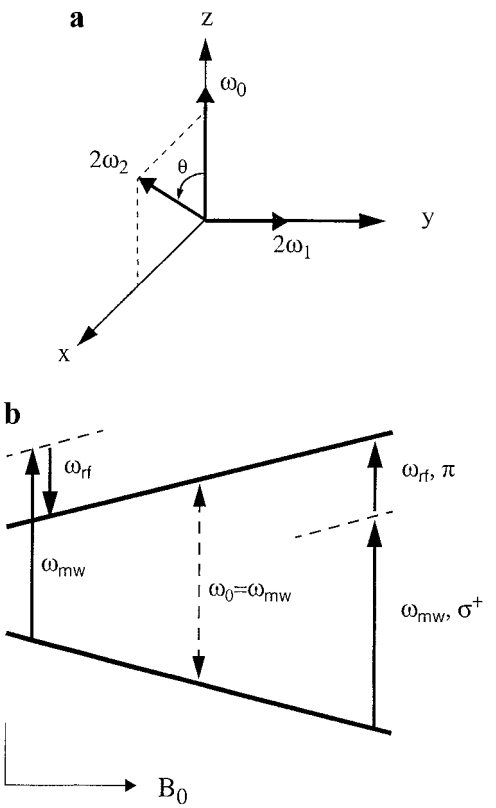

FIG. 5. Multiphoton resonances created with an mw and an rf field. (a) Field configuration in the laboratory frame used in experiments for the detection of multiphoton electron spin echoes. The fields are represented by respective angular frequencies: static field $\mathbf{B}_0$ by ω_0; mw field by ω_1; rf field by ω_2. (b) Energy level diagram showing two-photon resonances when the difference between the electron Larmor frequency ω_0 and the mw frequency ω_{mw} equals ω_{rf}.

$$\mathcal{H}''(t) = \omega_{\text{eff}} S_z'' + 2\omega_2 \cos(\omega_{\text{rf}} t)(\cos(\psi) S_z'' - \sin(\psi) S_y''). \quad [21]$$

A comparison of the Hamiltonians in Eqs. [1] and [21] indicates that the situation in the doubly primed frame is similar to that described above when the single-frequency oscillating field is tilted from the direction of the static field. In the doubly primed frame the rf field has *y* and *z* components that depend on the angle ψ. This angle is determined by the mw field strength and the frequency off-set from the single-photon resonance. In the doubly primed frame, and using the theory described above, approximate equations can be derived for the effective field strengths of $\omega_{\text{eff}}^{(1d)}$ and $\omega_{\text{eff}}^{(2d)}$ of the single- and two-photon rf resonances. With the resonance conditions $\Omega_S \approx \omega_{\text{rf}}$ and $\Omega_S \approx 2\omega_{\text{rf}}$, we find

$$\omega_{\text{eff}}^{(1d)} \propto \frac{\omega_1 \omega_2}{\omega_{\text{rf}}}, \quad [22]$$

$$\omega_{\text{eff}}^{(2d)} \propto \frac{\omega_1 \omega_2^2}{\omega_{\text{rf}}^2}. \quad [23]$$

These resonances occur between the states of the spin system which absorb mw photons, i.e., between dressed states. In the laboratory frame they will manifest as two- and three-photon resonances symmetric to the single mw photon transition, when the frequency offset $|\Omega_S|$ approximately equals ω_{rf} and $2\omega_{\text{rf}}$. An example of such two-photon resonances is shown in Fig. 5b. When the rf field is tilted from $\mathbf{B}_0$ ($\theta \neq 0°$), the *y* and *z* components of the rf field in the doubly primed frame decrease, as one can see by comparing the Hamiltonians in Eqs. [20] and [21]. Thus, with the field configuration shown in Fig. 5a one can expect to observe spectra consisting of even and odd resonances, which will disappear as the angle θ approaches 90°.

The creation of two-photon echoes is demonstrated at *Q*-band frequencies on a γ-irradiated quartz sample at a temperature of 100 K. The broad bandwidth of the *Q*-band resonator allows one to have very similar conditions for excitation and detection of both the low- and high-field two-photon echoes (see Fig. 5b). The low temperature is used to compensate for the small size of the sample (1.6-mm sample tube), which results in a poor signal-to-noise ratio. The echo-detected field-swept EPR spectrum obtained with a primary echo sequence with pulse lengths of 20 and 40 ns is shown in Fig. 6. It consists of a single narrow line with a full width of about 42 MHz at 1% of the maximum signal intensity. The signal is above the noise level up to a width of about 56 MHz. To avoid any influence of side lobes in the excitation spectrum of the pulses on our data, mw pulse lengths of 100 and 200 ns were used for the multiphoton experiments. The signal of the conventional echo

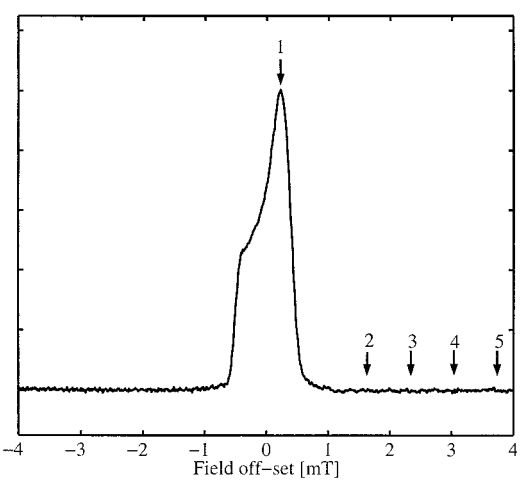

FIG. 6. Echo-detected single-photon EPR spectrum of γ-irradiated quartz measured at *Q*-band frequencies, temperature 100 K. The parameters for the echo sequence $\pi/2$–τ–π were $t_{\pi/2}$ = 20 ns, t_π = 40 ns, and τ = 400 ns. The arrows indicate positions where echo signals were measured. (1) Observer position for the single-photon echo experiment. (2–5) Observer positions for the two-photon echo measurements.

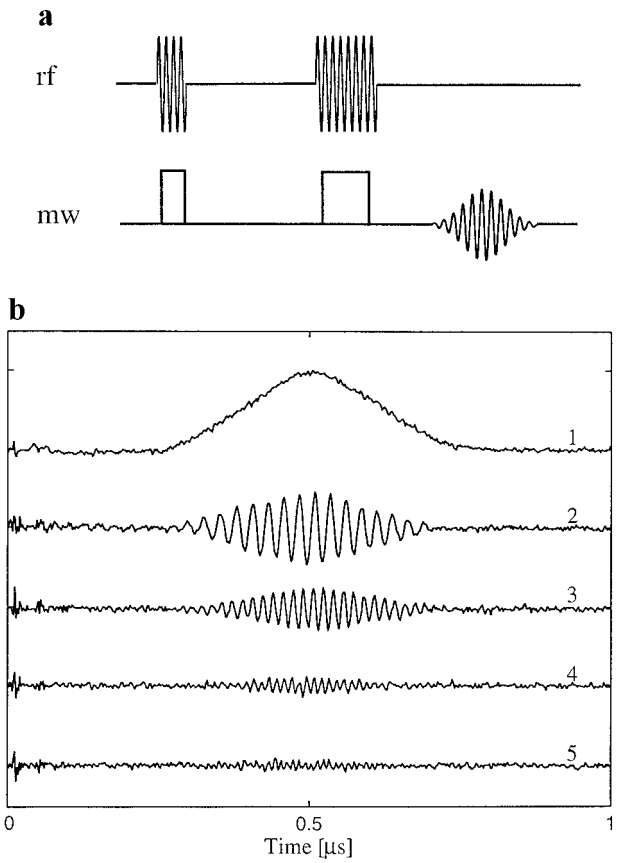

FIG. 7. (a) Pulse sequence used in multiphoton experiments. (b) Observed time-domain echo signals. (1) Single-photon echo, $\nu_0 = \nu_{mw}$, $\nu_1 = 2.5$ MHz. (2–5) Echoes measured at $\Delta = \nu_0 - \nu_{mw}$, with (2) $\Delta = 37.8$ MHz, (3) 58.2 MHz, (4) 78.4 MHz, and (5) 97.4 MHz. The field strength in the two-photon experiments was $\nu_1 \approx \nu_2 \approx 10$ MHz; the pulse lengths were 100 and 200 ns. Field positions for the measurements of the signals are indicated in Fig. 6. Traces (1–5) represent single-shot measurements.

was maximum for an mw field strength of about $\nu_1 = 2.5$ MHz[2] with these pulses (Fig. 7b, trace 1).

The pulse sequence for the creation of the multiphoton echoes is shown in Fig. 7a. The rf field was oriented along $\mathbf{B}_0$ ($\theta = 0$), and mw and rf amplitudes were approximately equal, $\nu_1 \approx \nu_2 \approx 10$ MHz. The rf and mw sources were not phase locked, and single-shot measurements were performed to avoid signal jittering. The echo traces 2–5 in Fig. 7b were obtained at fields corresponding to off-sets Δ of 37.8, 58.2, 78.4, and 97.4 MHz (see labels in Fig. 6), which were very close to the ν_{rf} values used in the experiments, namely 40, 60, 80, and 100 MHz. At each of these field positions the echo amplitudes were found to be maximum. A trend was observed that for each particular frequency ν_{rf}, the echo amplitude reaches a maximum at an off-set Δ which is less than this frequency. The echoes were observed under the condition that the field strengths ν_1 and ν_2 are too small to excite a single-photon echo even at the minimum off-set of 40 MHz. For $\nu_{rf} = 40$ MHz this condition is equal to that used for the numerical simulation shown in Fig. 4d. Off-resonance effects, which could be caused by the strong mw field alone were not observed under the conditions used in these experiments.

It was found experimentally that at $\nu_1 \approx \nu_2 \approx 10$ MHz and $\nu_{rf} = 40$ MHz (Fig. 7b, trace 2) the condition of the echo formation is close to optimum and the echo amplitude comparable with the amplitude of the single-photon echo (Fig. 7b, trace 1). The echo signals at higher off-sets Δ and the same field strengths of 10 MHz (traces 3–5) are lower than their maximal values. For an off-set of 80 MHz echo maxima were observed with $\nu_1 \approx \nu_2 \approx 15$ MHz and pulse lengths of 100 and 200 ns, and with $\nu_1 \approx \nu_2 \approx 10$ MHz and pulse lengths of 200 and 400 ns. Furthermore, it was found that the amplitude of the echoes is maximum when the ratio $(\nu_1\nu_2)/\Delta$ is equal to the value of ν_1 used in the single-photon echo experiment.

The echo-detected two-photon EPR spectra for $\nu_{rf} = 40$ and 80 MHz are shown in Figs. 8b, c. The spectra were obtained by Fourier transformation of the time-domain traces and represent the behavior of the signal amplitudes at 40 and 80 MHz. As a reference, the single-photon spectrum was recorded with the same sequence (Fig. 8a). For each experiment optimized field strengths were used, $\nu_1 = 2.5$ MHz and $\nu_2 = 0$ MHz for the single-photon echo, $\nu_1 \approx \nu_2 \approx 10$ MHz for $\nu_{rf} = 40$ MHz, and $\nu_1 \approx \nu_2 \approx 15$ MHz for $\nu_{rf} = 80$ MHz for the two-photon echoes. The two-photon spectra with shapes that are exact replicates of the single-photon spectrum are symmetrically placed to the position of the latter. The observed peak-to-peak splittings of the two-photon spectra (Figs. 8b, c) are close to twice the radio frequencies of 40 and 80 MHz.

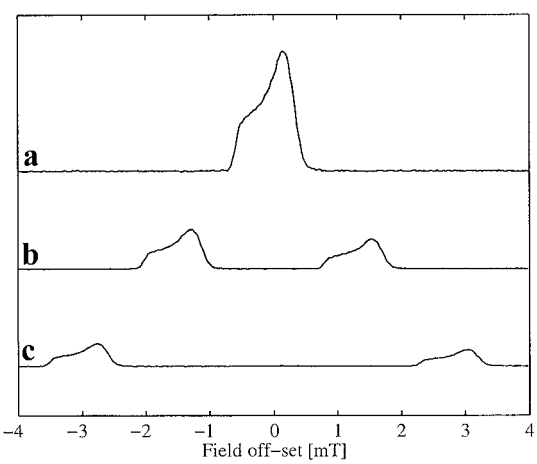

FIG. 8. Echo-detected single- and two-photon spectra of γ-irradiated quartz. (a) Single-photon spectrum, $\nu_1 = 2.5$ MHz. (b) Two-photon spectrum with $\nu_{rf} = 40$ MHz, $\nu_1 \approx \nu_2 \approx 10$ MHz. (c) Two-photon spectrum with $\nu_{rf} = 80$ MHz, $\nu_1 \approx \nu_2 \approx 15$ MHz. A sequence with pulse lengths of 100 and 200 ns was used. The spectra were obtained by Fourier transformation of the time-domain traces and represent the behavior of the signal amplitude at 0, 40, and 80 MHz, as a function of the static magnetic field.

[2] Actual frequencies and amplitudes used in the experiments are denoted by ν_{mw}, ν_{rf}, ν_1, ν_2, and Δ with $2\pi\nu = \omega$ and $2\pi\Delta = \Omega_S$.

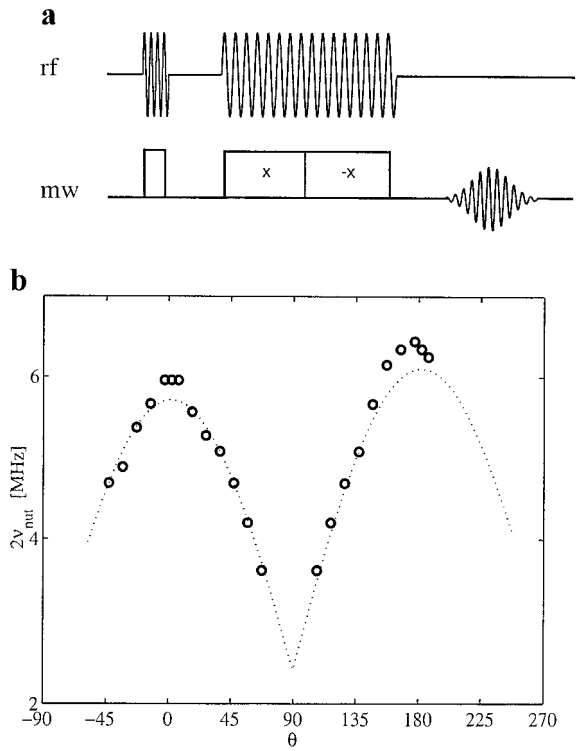

FIG. 9. Two-photon nutation experiments. (a) Pulse sequence used for measuring the electron nutation frequency under combined mw and rf radiation. (b) Nutation frequency as a function of the angle between the rf field and $\mathbf{B}_0$. The dashed line represents the function $|\cos(\theta)|$.

The two-photon echoes disappeared when the rf field was switched off or oriented perpendicular to $\mathbf{B}_0$. To demonstrate the dependence of the observed signals on the orientation of the rf field with respect to $\mathbf{B}_0$, the nutation frequencies under the combined mw and rf field excitation were measured as a function of the angle θ. The room temperature measurements were performed at *X*-band using a modified PEANUT sequence (Fig. 9a), which creates a rotary echo at the mw frequency (*39*). The length of the second mw and rf pulse was 5.12 μs with amplitudes of $\nu_1 \approx 11$ MHz and $\nu_2 \approx 10$ MHz; the length of the $\pi/2$ pulse was 200 ns. For the single-photon transition (rf off, $\nu_{mw} = \nu_0$), a nutation frequency of $2\nu_{nut} \approx 22$ MHz was found. In the two-photon experiments with $\nu_{rf} = 25$ MHz the electron spin Larmor frequency was displaced from ν_{mw} by 25 MHz. The width of the EPR line at the 1% level was about 11 MHz. A phase-sensitive detector was used for signal demodulation. Figure 9b shows the nutation frequencies $2\nu_{nut}$ measured as a function of the angle θ. The nutation frequencies $2\nu_{nut}$ were found to be proportional to the modulus of $\cos(\theta)$ (dotted line in Fig. 9b) and, thus, proportional to the projection of the rf field onto the *z* axis. The echo signal disappeared for angles θ close to 90°.

The dependence of the echo amplitude on $\nu_1\nu_2$ and the line positions and the dependence of the nutation frequency on angle θ verify that the observed signals are two-photon echoes, which are created when one mw and one rf photon are simultaneously absorbed or emitted by the spin system. In the doubly primed frame, these transitions can be considered as single rf photon processes or as a transition between dressed states.

The theory also predicts multiphoton transitions where more than one rf photon is involved. To prove the existence of such transitions, the echo experiments were carried out at higher field strengths, namely $\nu_1 \approx \nu_2 \approx 14$ MHz, and an rf of 30 MHz. A 2D spectrum obtained with the two-pulse echo sequence (Fig. 7a) with mw and rf pulses of lengths 100 and 200 ns and the rf field along *z* is shown in Fig. 10. One dimension represents the field off-set from the center of the single-photon transition; the other dimension represents the Fourier transform (absolute value) of the time-domain echo signals. Apart from the strongly distorted and broadened single- and two-photon echoes centered at (0, 0) and at ($\pm$1.1 mT, $\pm$30 MHz), new signals appeared at about ($\pm$2.1 mT, $\pm$59 MHz), i.e., at field and frequency off-sets that are twice as large as those of the two-photon echoes. The new signals were very weak and disappeared when the rf field vector was rotated from the *z* axis. Moreover, the signal amplitude of these new features decreased more rapidly than those of the two-photon echoes when the strength of the rf field was reduced. This behavior indicates that these signals represent three-photon transitions involving one mw photon and two rf photons.

The amplitudes of the single-, two-, and three-photon echoes as a function of ν_1 and ν_2 are shown in Fig. 11. For both the two- and three-photon echoes, data with a variable ν_1 and a fixed ν_2 value, and vice versa, are given. The amplitudes of the different types of echoes reached their maxima at different field strengths. The maximum amplitudes were used as initial points in the plots (0 dB in Fig. 11). For the single- and two-photon resonances the echo maxima could clearly be identified by using a two-pulse sequence with flip angles $\pi/2$ and π. For

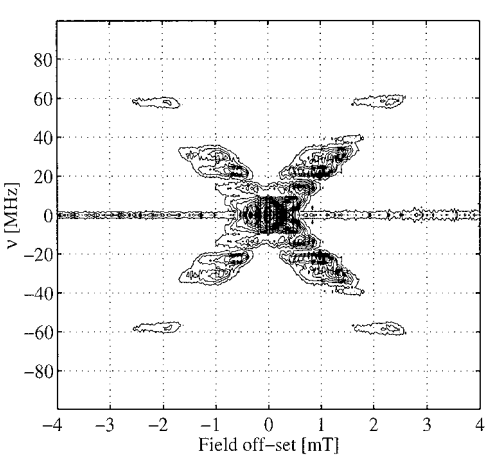

FIG. 10. Contour plot of the 2D spectrum, field off-set versus frequency off-set. $\nu_{rf} = 30$ MHz; $\nu_1 \approx \nu_2 \approx 15$ MHz. The peaks shifted by $\pm$59 MHz and $\pm$2.1 mT from the center (0, 0) are three-photon resonances.

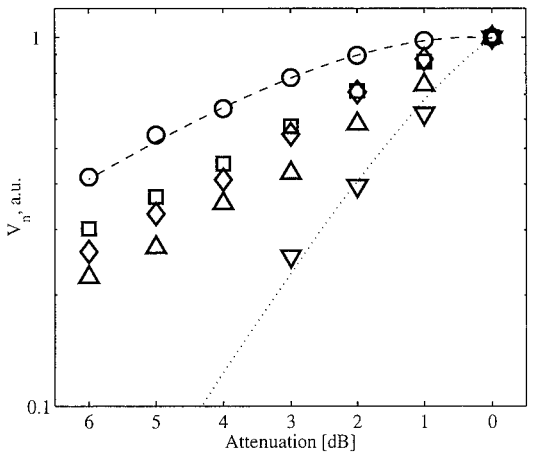

FIG. 11. Single- and multiphoton echo amplitudes as a function of the mw and rf field strengths. Single-photon echoes versus ν_1 (○); two-photon echoes at $\nu_{rf} = 40$ MHz as function of ν_1 (◇) and ν_2 (□); three-photon echoes at $\nu_{rf} = 30$ MHz as function of ν_1 (△) and ν_2 (▽). Fit of the experimental data by the function $\sin(\theta_1)\sin^2(\theta_2/2)$, with $\theta_2 = 2\theta_1$. Dashed line, $\theta_1 \propto \nu_1$; dotted line, $\theta_1 \propto \nu_2^2$.

three-photon transitions the maximum echo amplitude could not be observed with the available field strength, but it was not far from its optimum. The amplitude of the single-photon echo follows the function $\sin(\theta_1)\sin^2(\theta_2/2)$ (*40*), where θ_1 and θ_2 are the flip angles of the first and second pulse and $\theta_2 = 2\theta_1$ (dashed line in Fig. 11 with $\theta_1 \propto \nu_1$). The amplitudes of the two-photon echoes show virtually the same behavior as a function of both ν_1 and ν_2.

The three-photon echoes behave in a different way. An attenuation of ν_2 by 3 dB reduced the echo amplitude by almost the same amount as an attenuation of ν_1 by 6 dB. The weak signal, the rapid decay of the signal intensity as a function of the rf amplitude, and the demands of the echo method allow only qualitative conclusions about the three-photon echoes. Nevertheless, a corresponding fit of the experimental data indicates (dotted line in Fig. 11 with $\theta_1 \propto \nu_2^2$) that the flip angle θ_1 is proportional to ν_2^2.

From the observed dependences we conclude that for the two-photon echoes the relation between flip angle and field strength is given by $\theta_1 \propto \nu_1\nu_2$ and for the three-photon echoes by $\theta_1 \propto \nu_1\nu_2^2$.

DISCUSSION

The results for the two-photon transitions given in Eqs. [18] and [19] obtained by Floquet theory and those obtained by the Bloch equations in the doubly rotating frame (*30*) show the same dependence of the effective field and the level shifts on the strength and the frequency of the radiation field. In EPR spectroscopy these dependences were initially proved by monitoring the spin nutation at the second harmonic of the single-frequency excitation field (*27*). Our experimental results obtained with two-frequency excitation (mw and rf), which is more convenient for practical applications, are in agreement with those reported in (*27*). Thus Floquet theory, implemented in this work for even multiphoton resonances, can be applied to further investigate the spin dynamics during this kind of transition.

The experimental echo-detected two-photon spectra of γ-irradiated quartz show the same features as that reported for the two-photon cw absorption spectra of free radicals measured with the same field geometry (*14*), namely lines at positions $\omega_0 \approx \omega_{mw} \pm \omega_{rf}$. The cw spectra were measured at much lower mw and rf power and smaller frequency off-sets. The signal intensities were found to be depended on T_1 and could not always be observed for radicals at room temperature. In our experiments strong two-photon echoes of irradiated quartz were observed at room temperature ($T_1 \approx 0.2$ ms at *Q* band), indicating that by using an intrinsically nonlinear method for excitation, multiphoton transitions can easily be studied.

Compared to the two-photon electron spin-echo experiments where the echo was excited by a single mw field at frequency $\omega_{mw} = \omega_0/2$, tilted from $\mathbf{B}_0$ by 45°, and detected at the second harmonic $2\omega_{mw}$ (*26*), we used for excitation two radiation fields that differ in frequency by a factor 500–1000. This allows stronger effective fields to be used for the two-photon transitions (compare (*26, 27*) with the results presented in this work). Moreover, the experiments with mw and rf radiation can be carried out with a much simpler experimental setup than that described in (*26*), namely with an ENDOR probe head rotated by 90°. In pulse dressed EPR experiments (*28*), a similar technique was used but the mw frequency was on resonance with the electron Larmor frequency, and single rf photon absorption (or echo signal) was monitored at the single mw photon transition. In our study, excitation and detection are performed using two- and three-photon transitions, making another aspect of the dressed states concept clearly visible, namely that these states can play the role of intermediate states for multiphoton transitions.

CONCLUSION

In this work we have demonstrated that Floquet theory, up to now applied in magnetic resonance for the description of multiphoton transitions with an odd number of photons, can be extended to multiphoton transitions with an even number of photons. Electron spin-echo signals of two- and three-photon transitions were observed using an rf field oriented along the static magnetic field $\mathbf{B}_0$ and an mw field oriented perpendicular to $\mathbf{B}_0$. Theory and experiments demonstrate that with this field configuration multiphoton resonances can easily be observed in pulse EPR experiments.

In the following we propose some applications of multiphoton resonances excited by a transverse mw field and a longitudinal rf field. First of all it should be noted that in multiphoton experiments the frequencies are different for excitation and

detection. This allows one to perform experiments where pumping and observation take place at the same time. As an example, we propose to carry out coherent Raman beat EPR experiments (*41*) by using second-harmonic detection similar to how it was used for nutation experiments (*27*).

A second experiment we propose is related to the problem of coherence transfer between electron and nuclear spins. A close relation exists between the matched electron spin-echo envelope modulation approach (*42*) and the dressed spin experiment (*28*). In the former experiment, matching of the electron spin nutation frequency to the nuclear Larmor frequency allows for an effective coherence transfer during prolonged mw pulses. In the latter experiment the resonance frequency of the electron spin under a similar condition was directly measured, demonstrating that the energy levels are shifted, so that the resonance of the electron spins can be observed at radio frequencies. The present multiphoton approach could be an alternative way to produce a pattern of energy levels appropriate for a resonant coherence transfer between electron and nuclear spins. In this approach the energy levels of the dressed spins are determined by the mw and rf frequencies and only the shifts of the levels depend on the field strength.

The last proposed experiment is related to *multilevel* spin systems. Since multiphoton transitions with $\Delta m > 1$ can be induced between pure states of the system, they could be used to obtain data which cannot be deduced from conventional EPR of a multilevel system.

EXPERIMENTAL

The experiments were performed on two homebuilt pulse EPR spectrometers of similar design operating at 35.3 GHz (*Q* band) (*43*) and 9.62 GHz (*X* band) (*44*). Both instruments are equipped with four mw pulse-forming channels and with high-power TWT amplifiers (ASE 187 Ka, 100 W at *Q* band, and ASE 117X-1, 1 kW at *X* band). A Varian E110 bridge was used as an mw source at 35.3 GHz and an mw synthesizer (Wiltron, 6722B) at 9.62 GHz. The static magnetic field B_0 was measured with an NMR gaussmeter (Bruker, ER 035M). Bruker ENDOR probe heads were used for both frequency bands (probe head ER 5106 QTE, with a TE_{013} cylindrical cavity at *Q* band, and probe head ER 4118X-MD-4-W1, with a TE_{011} dielectric ring resonator at *X* band). The *Q*-band probe head was modified by Bruker to allow for measurements in the frequency range of the Varian microwave bridge.

Low-loss coaxial cables were used to connect the probe head with the mw bridge to allow for an easy change of the relative orientation between the direction of the rf field and $\mathbf{B}_0$. The rf pulses were created by switching the cw signal of an arbitrary wave function generator (LeCroy, LW420) and a signal generator (Marconi, 2022), and were amplified by high-power rf amplifiers (Kalmus 137C, and Amplifier Research 100LB8). The spectral purity of the mw and rf radiation was checked with a spectrum analyzer (Hewlett Packard, HP 8565E). The Kalmus amplifier had a relatively strong second harmonic, which could create unwanted spectral features at higher rf power. By adding a corresponding low-power rf signal in antiphase, the intensity of the second harmonic at the output of the amplifier could be reduced by about -35 dBc. The other devices did not produce any unwanted signals, which could manifest in effects similar to those observed in the experiments.

The strengths of the mw and rf fields were measured via the nutation frequencies of the electron spins and the nuclear spins of the protons. PEANUT experiments were performed to determine the nutation frequencies of the electron spins (*39*). At *Q* band the rf field strengths were determined via the proton nutation frequencies measured in a Mims-ENDOR experiment; at *X* band they were measured with a calibrated pick-up coil. In addition, the mw field strengths were checked during the experiments by observing the echo amplitude as a function of the incident power. The variations in the mw field strengths were smaller than 10%.

Quartz glass (Herasil) γ-irradiated with 90 kGy was used to demonstrate the multiphoton effects. Some of the measurements were performed at low temperature (100 K) using a cooling system from Oxford Inc. To separate single- and multiphoton signals from each other, analog phase-sensitive detection or digital signal processing (DSP) was used. In the former case the signals were mixed with the reference signal in a double-balanced mixer (Mini Circuits, ZAD-1-1) and then digitized. In the DSP method the time-domain traces were digitized at 500 MS/s with an oscilloscope (LeCroy, LC534) and then Fourier transformed.

ACKNOWLEDGMENTS

This research has been supported by the Swiss National Science Foundation. The authors thank S. Stoll for the fast algorithm to build Floquet matrices and M. Kälin and Dr. J. Harmer for helpful discussions. The technical assistance by J. Forrer is gratefully acknowledged.

REFERENCES

1. C. Cohen-Tannoudji, J. Dupont-Roc, and G. Grynberg, "Atom–Photon Interaction: Basic Processes and Application," Wiley, New York (1992).
2. M. Göppert-Mayer, *Ann. Phys. (Leipzig)* **5,** 273–294 (1931).
3. M. Ito and N. Mikami, *Appl. Spectrosc. Rev.* **16,** 299–352 (1980).
4. W. Anderson, *Phys. Rev.* **104,** 850–851 (1956).
5. J. I. Kaplan and S. Meiboom, *Phys. Rev.* **106,** 499–501 (1957).
6. P. P. Sorokin, I. L. Gelles, and W. V. Smith, *Phys. Rev.* **112,** 1513–1515 (1958).
7. J. W. Orton, P. Auzins, and J. E. Wertz, *Phys. Rev. Lett.* **4,** 128–129 (1960).
8. M. Rudin, A. Schweiger, and Hs. H. Günthard, *J. Magn. Reson.* **51,** 278–285 (1983).
9. S. A. Al'tshuler and B. M. Kozyrev, "Electron Paramagnetic Resonance in Compounds of Transition Elements," Wiley, New York (1974).

10. C. Cohen-Tannoudji, Optical pumping and interactions of atoms with electromagnetic field, *in* "Cargese Lectures in Physics" (M. Lévy, Ed.), Vol. 2, pp. 347–393, Gordon and Breach, New York (1968).
11. J. Margerie and J. Brossel, *C. R. Acad. Sci. (Paris)* **241,** 373–375 (1955).
12. J. Winter, *C. R. Acad. Sci. (Paris)* **241,** 375–377 (1955).
13. R. Boscaino, I. Ciccarelo, C. Cusumano, and M. W. P. Strandberg, *Phys. Rev. B* **3,** 2675–2682 (1971).
14. J. Burget, M. Odehnal, V. Petříček, J. Šácha, and L. Trlifaj, *Czech. J. Phys. B* **11,** 719–728 (1961).
15. P. Bucci, M. Martinelli, and S. Santucci, *J. Chem. Phys.* **53,** 4524–4531 (1970).
16. F. Chiarini, M. Martinelly, L. Pardi, and S. Santucci, *Phys. Rev. B* **12,** 847–852 (1975).
17. F. Bloch and A. Siegert, *Phys. Rev.* **57,** 522–527 (1940).
18. J. S. Hyde, P. B. Sczaniecki, and W. Froncisz, *J. Chem. Soc. Faraday Trans.* **85,** 3901–3912 (1989).
19. P. B. Sczaniecki, J. S. Hyde, and W. Froncisz, *J. Chem. Phys.* **94,** 5907–5916 (1991).
20. H. S. Mchaourab and J. S. Hyde, *J. Chem. Phys.* **98,** 1786–1796 (1993).
21. M. Jelen and W. Froncisz, *J. Chem. Phys.* **109,** 9272–9279 (1998).
22. D. G. Gold and E. L. Hahn, *Phys. Rev. A* **16,** 324–326 (1977).
23. Y. Zur and S. Vega, *J. Chem. Phys.* **79,** 548–558 (1983).
24. Y. Zur, M. H. Levitt, and S. Vega, *J. Chem. Phys.* **78,** 5293–5310 (1983).
25. E. M. Krauss and S. Vega, *Phys. Rev. A* **34,** 333–350 (1986).
26. R. Boscaino and F. M. Gelardi, *Phys. Rev. B* **46,** 14550–14558 (1992).
27. R. Boscaino, F. M. Gelardi, and G. Messina, *Phys. Rev. B* **33,** 3076–3082 (1986).
28. G. Jeschke, *Chem. Phys. Lett.* **301,** 524–530 (1999).
29. F. H. M. Faisal, "Theory of Multiphoton Processes," Plenum Press, New York (1992).
30. R. Boscaino and G. Messina, *Physica C* **138,** 179–187 (1986).
31. M. Jelen and W. Froncisz, *J. Chem. Phys.* **108,** 4563–4571 (1998).
32. F. Persico and G. Vetri, *Phys. Rev. B* **8,** 3512 (1973).
33. J. H. Shirley, *Phys. Rev. B* **138,** B979–987 (1965).
34. T. O. Levante, M. Baldus, B. H. Meier, and R. R. Ernst, *Mol. Phys.* **86,** 1195–1212 (1995).
35. S. Vega, Floquet theory, *in* "Encyclopedia of Nuclear Magnetic Resonance" (D. M. Grant and R. K. Harris, Eds.), pp. 2011–2025, Wiley, Chichester (1996).
36. T. S. Ho, S. I. Chu, and J. V. Tiets, *J. Chem. Phys. Lett.* **96,** 464–471 (1983).
37. H. T. Davis, "Introduction to Nonlinear Differential and Integral Equations," Dover, New York (1962).
38. H. Salwen, *Phys. Rev.* **99,** 1274–1286 (1955).
39. S. Stoll, G. Jeschke, M. Willer, and A. Schweiger, *J. Magn. Reson.* **130,** 86–96 (1998).
40. W. Mims, Electron spin echoes, *in* "Electron Paramagnetic Resonance" (S. Geschwind, Ed.), pp. 263–351, Plenum Press, New York (1972).
41. M. K. Bowman, *Isr. J. Chem.* **32,** 339 (1992).
42. G. Jeschke and A. Schweiger, *J. Chem. Phys.* **105,** 2199–2211 (1996).
43. J. J. Shane, R. Rakhmatouline, J. Forrer, and A. Schweiger, *Proceed. of 39th Rocky Mountain Conference on Analytical Chemistry, Denver,* p. 133 (1995).
44. Th. Wacker, Ph.D. Thesis, ETH, Zurich, No. 9913 (1992).